Available online at www.sciencedirect.com
SCIENCE DIRECT®
Nuclear Instruments and Methods in Physics Research A 544 (2005) 225–235
NUCLEAR INSTRUMENTS & METHODS IN PHYSICS RESEARCH Section A
www.elsevier.com/locate/nima

Neutralized transport experiment

P.K. Roy[a,*], S.S. Yu[a], S. Eylon[a], E. Henestroza[a], A. Anders[a], E.P. Gilson[b], F.M. Bieniosek[a], W.G. Greenway[a], B.G. Logan[a], W.L. Waldron[a], D.B. Shuman[a], D.L. Vanecek[a], D.R. Welch[c], D.V. Rose[c], C. Thoma[c], R.C. Davidson[b], P.C. Efthimion[b], I. Kaganovich[b], A.B. Sefkow[b], W.M. Sharp[d]

[a]*Lawrence Berkeley National Laboratory, Berkeley, California 94720, USA*
[b]*Princeton Plasma Physics Laboratory, Princeton, New Jersey 08543-0451, USA*
[c]*Mission Research Corporation, Albuquerque, New Mexico 87110-3946, USA*
[d]*Lawrence Livermore National Laboratory, Livermore, California 94550, USA*

Available online 2 March 2005

Abstract

Experimental details on providing active neutralization of high brightness ion beam have been demonstrated for Heavy Ion Fusion program. A K^+ beam was extracted from a variable–perveance injector and transported through 2.4 m long quadrupole lattice for final focusing. Neutralization was provided by a localized cathode arc plasma plug and a RF volume plasma system. Effects of beam perveance, emittance, convergence focusing angle, and axial focusing position on neutralization have been investigated. Good agreement has been observed with theory and experiment throughout the study.

PACS: 52.59.Bi,Fn; 29.27.−a; 52.40.Mj; 41.75.Fr,Ht; 29.27.−a

Keywords: Beam transport; Neutralization; Plasma; Diagnostic

1. Introduction

Intense beam focusing and neutralization for final focus are much of great interest for the Heavy ion fusion (HIF) [1–3] program. Neutralized ballistic transport (NBT) [4–11] is presently being studied for propagating intense heavy ion beams inside a reactor chamber to an inertial confinement fusion (ICF) target. The present generation of indirect-drive targets requires a total particle current exceeding 40 kA (requires beam energy of 6 to 6.5 MJ) divided roughly between a hundred beams, each beam of 2 mm focal spot radius. A recent HIF driver study [12] demonstrates that stringent final-focus requirements [13–15] can be

*Corresponding author. LBNL, MS#47R 0112, 1 Cyclotron Road, Berkeley, CA-94720, USA. Tel.: +1 510 495 2616; fax: +1 510 486 5392.
E-mail address: PKRoy@lbl.gov (P.K. Roy).

0168-9002/$ - see front matter © 2005 Elsevier B.V. All rights reserved.
doi:10.1016/j.nima.2005.01.210

met, provided that active neutralization is implemented to overcome the formidable space charge of the intense ion beams. In the NBT scheme, the individual beams focus outside the target chamber and enter through ports in the chamber walls. These beams are focused and directed such that they intersect before striking the target and then strike the target as they are expanding into an annular configuration [15]. The target chamber is filled at low pressure with gas, such as flibe. A volumetric plasma is produced as the flibe gas is partially ionized by the beam as well as by X-rays emitted by the hot target. This volumetric plasma is not adequate to provide the necessary neutralization. Therefore, additional plasma, the "plasma plug," is externally injected outside the chamber entry port, through which the beam passes. Chamber transport using annular and filled plasma regions in the transport chamber has been examined numerically by several investigators [16–18]. To quantitatively evaluate the various mechanisms for neutralization, the Neutralized Transport Experiment (NTX) was constructed at Lawrence Berkeley National Laboratory. In this NTX experiment, an initially non-neutralized ion beam is passed through a finite thickness of plasma (from a plasma plug). Plasma electrons are dragged for partial charge and current neutralization, reducing the size of beam spot. Partially neutralized, the beam is also transported through a volumetric plasma region for further neutralization to make a small spot.

Technical issues of high brightness beam extraction and transport, physics issues of neutralized beam size, as well as comparison between theory and experiment results are presented in this article.

2. Technical and physics issues

Extraction of a high brightness uniform ion beam from an injector, its transport through quadrupoles to make converging beam optics for the drift through the final focus and neutralization in the final focus section to make a mm size beam spot depends on several technical and physical issues as described in the following sub-section.

2.1. Extraction of a high brightness ion beam

A uniform high brightness ion beam depends on optimal emission temperature, smooth source surface, and aperturing, as well as an effective design of the injector. NTX ion beam extraction is well equipped with all of these considerations which gives injection energy, current and ion species.

2.2. Beam perveance

The key scaling parameter for beam transport is the dimensionless perveance, defined as a ratio proportional to the beam space charge potential energy, divided by kinetic energy ($K = 2I_b/I_A\ \beta_i^2$, where $I_A = \beta_i\gamma_i m_i c^3/eZ$ is the Alfven current with a beam of current velocity $\beta_i c$, and relativistic factor γ_i). The larger space charge associated with higher perveance has important ramifications for a HIF driver [19]. Since, the perveance is proportional to the ratio of the potential energy to the kinetic energy of the beam, we can access driver-relevant physics with low-energy beams as long as the experimental perveance values are driver relevant. Early analytic work by Olson [20] estimated that the upper perveance limit for ballistic transport $K \cong 1.6 \times 10^{-5}$. Recent designs typically require a few times 10^{-4}. The NTX beam source is designed to produce a maximum current of 75 mA, corresponding to a perveance of about $\sim 10^{-3}$.

2.3. Convergence angle and emittance

The envelope equation predicts the radius of the beam for a given convergence angle from the last focusing element. Approximately, beam radius (r) depends on convergence angle (θ) through the relation $r \cong \varepsilon/\theta$, where ε is the emittance. Sources of emittance growth are geometric aberration, magnetic transport mismatch and incomplete neutralization. The latter two were overcome with careful design of the experiment. Though beam spot size is a function of emittance for emittance-dominated focus, convergence angle also plays a role. Larger angle of the convergence can make a small spot if emittance growth is not too large.

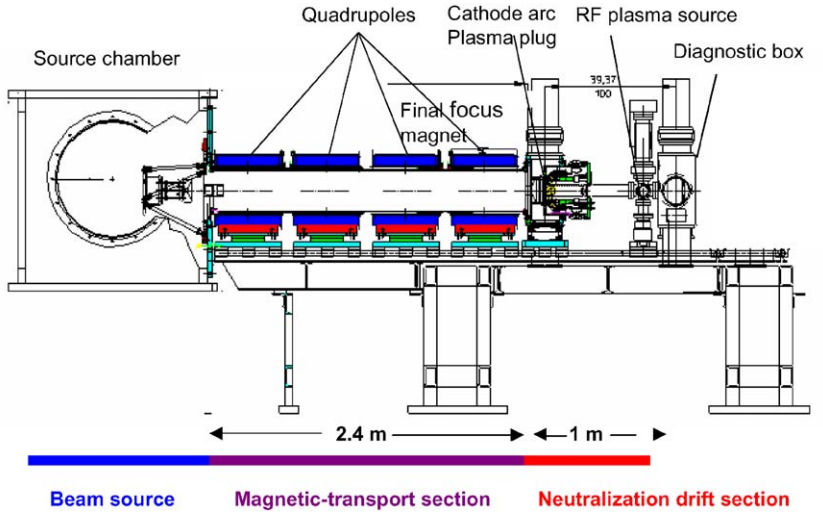

Fig. 1. A schematic of NTX beam line.

2.4. Optimization of neutralization

Reduction of the beam size at the target depends on the entire neutralization system. This system consists of optimum beam energy, axial focus length, plasma parameters and implementation in real time of all optimum conditions during neutralization.

This paper provides experimental results in support of all of the above major issues.

3. Beam optics and focusing

Fig. 1 shows a sketch of the NTX beam line. A detailed description of the NTX construction and beam diagnostics has been given elsewhere [21]. In brief, the beam line consists of (1) an ion beam injector, (2) 4 quadrupole magnets and (3) a meter-long final focus drift section equipped with plasma sources and diagnostics.

3.1. Beam injector

The K^+ beam is produced by a standard hot-plate source [22], with the perveance being determined by passing the beam through a round metal aperture after the diode. Pulsed power is provided by a Marx generator that was used in the Multiple Beam Test Experiment (MBE-4) [23]. A timed crowbar switch on NTX produces pulses with 0.5–1 μs rise time and a 10 μs "flat-top". A diagnostic station downstream of the aperture assembly measures the current with a Faraday cup and measures the line-integrated beam profile and emittance at injection with a slit/slit-cup setup. Fig. 2(a) shows that a smooth uniform bright beam profile is generated by increasing source temperature, smoothing the source surface and positive biasing of the aperture. As the bias potential on the aperture was reduced, electron neutralization led to enhanced current density on-axis and a highly non-uniform beam profile was observed. The unapertured beam current follows the Child–Langmuir Law, reaching 80 mA at 400 keV. With a 2 cm diameter aperture, the current is reduced by approximately one half; a 1 cm diameter aperture reduces the current to 1/4 of the 2 cm aperture value. Most of the detailed experiments were performed with the 2 cm aperture, where the current was 25 mA at 300 keV. The line-integrated beam profile is parabolic, indicative of a uniform beam profile, and the normalized edge emittance is measured to be 0.05 πmm mr, which is less than a factor of 2 times of source-temperature-imposed value. The beam size, density, and emittance are in good agreement [21] with the EGUN prediction as shown in Fig. 3.

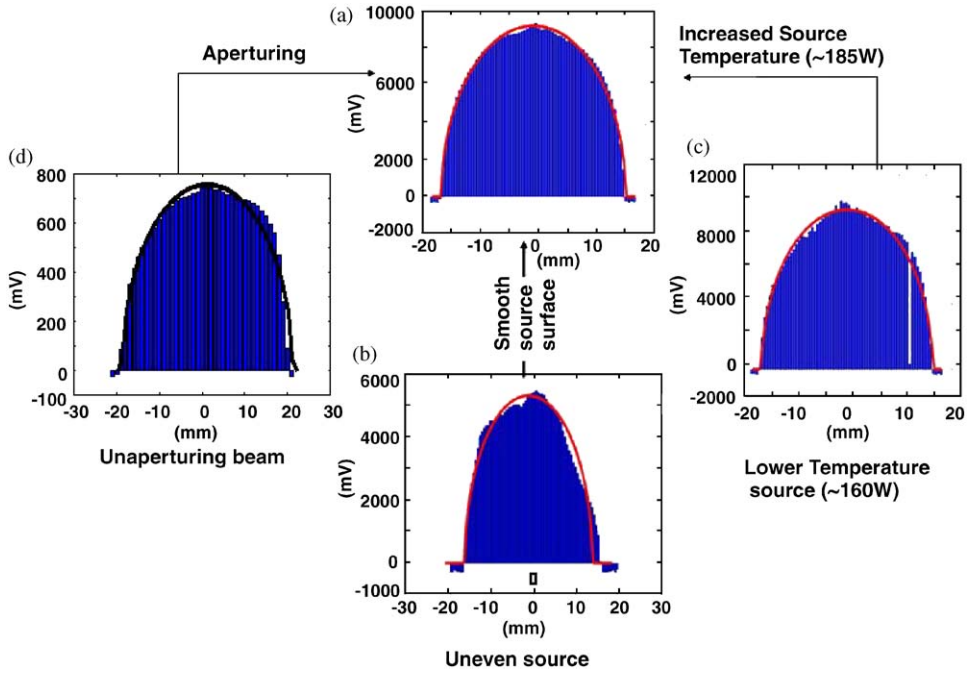

Fig. 2. Slit integrated NTX ion beam profile. Profile (a) was obtained by increasing source temperature, smoothing source surface and biasing aperture.

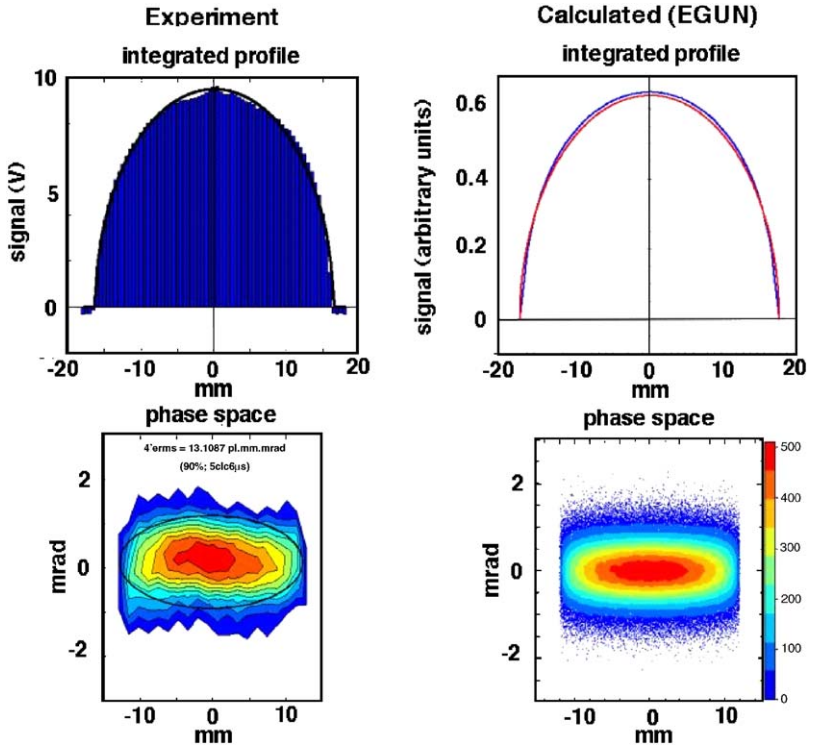

Fig. 3. A high brightness apertured beam (300 kV, 25 mA, 2 cm aperture).

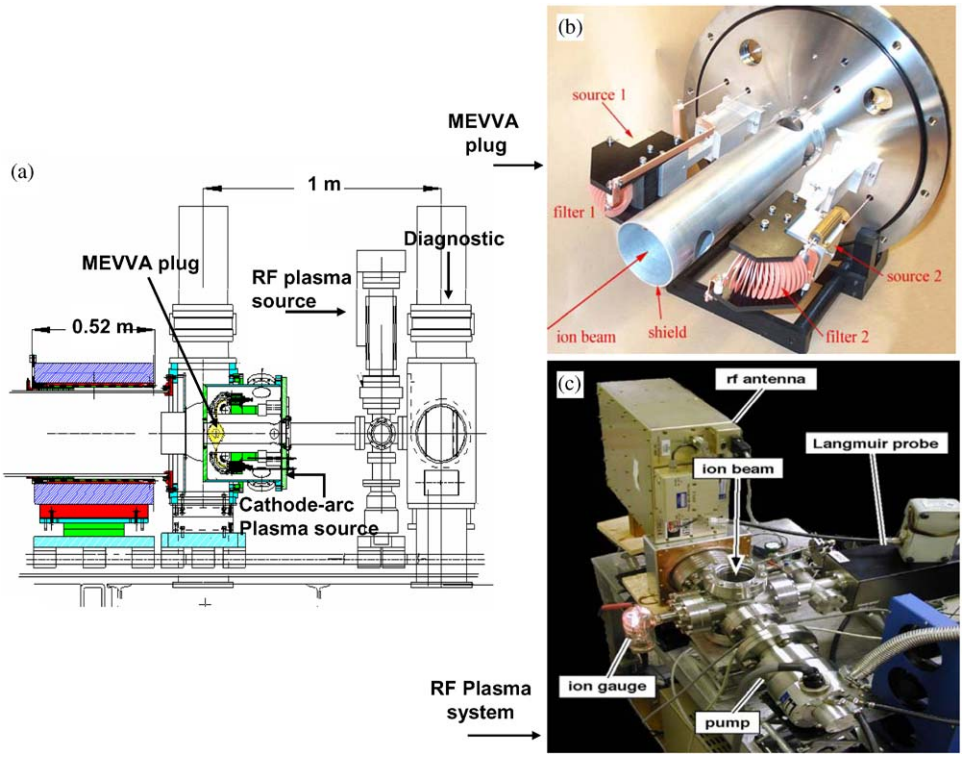

Fig. 4. A schematic of the 1 m long neutralization section with the location of the plasma sources, (b) cathode arc MEVVA plasma plug and (c) RF pulse volume plasma source.

3.2. Quadrupoles for beam focusing

Four pulsed quadrupoles, as shown in the Fig. 1, enclosing a thin wall stainless steel tube of 26 cm in diameter [24] are used in the NTX. The choice of a 60 cm half-lattice period and 2.4 m total length is a scaled version of a driver design. The quadrupole fields are chosen to obtain a beam with a large excursion of up to 10 cm in the magnetic lattice to reach an exit condition of 2 cm radius and 20 mr convergence at the entrance to the neutralization region.

3.3. Plasma sources and final drift section

Fig. 4 shows (a) schematic representation of a 1 m long neutralization section, equipped with a (b) Metal Vapor Vacuum Arc (MEVVA) plug and (c) RF plasma source. As focused from the last magnets, ions from the poorly matched beam head and halo ions in the main pulse of the beam can strike the outer wall of the transport tube. A single-ion impact can produce thousands of secondary electrons depending on the energy and angle of incidence [25,26] with ions of grazing-angle incidence producing the largest secondary electron yield [27]. If the secondary electrons are not stopped, they are attracted to the beam potential and can provide some degree of beam neutralization. A wall radius comparable to that of the beam will provide some sizable degree of neutralization and prevent the observation of expected "vacuum transport." In order to reduce partial uncontrolled neutralization, a positively biased liner mesh was installed inside the drift section and the non-neutralized beam size at the end of drift section was measured [28].

4. MEVVA plasma plug

Cathodic arcs are known to produce metal plasma from practically any metal of the periodic table: the cathode is the feedstock material [29]. If a cathodic arc plasma is used with ion extraction, the system is referred to as the MEVVA or Metal Vapor Vacuum Arc, ion source. For NTX, a plasma plug is required and hence only the cathodic arc plasma generator (without ion extraction) is used. In the literature, such generators are generally referred to as cathodic arc plasma sources or plasma guns [30]. Metal plasma is generated at cathode spots. It expands rapidly from the spot, with ions attaining supersonic velocity of about 1.5×10^4 m/s. The streaming metal plasma is injected in a curved solenoid (plasma filter) to remove any liquid or solid debris particles that are also produced at cathode spots [31]. As a side effect, neutral metal atoms are also removed from the streaming plasma. The filtered metal plasma represents the "plasma plug" in the current experiments.

The cathodic arc is powered by a 10-stage pulse forming network (PFN). The arc current, and thus plasma density, can be selected and tuned by the charging voltage of the PFN. For symmetry reasons, two arc sources produce plasma in such a way that the two plasma streams enter the ion beam region from opposite directions. This MEVVA plasma plug was characterized using a Scientific Systems Langmuir probe, and aluminum plasma density was measured as a function of space and PFN charging voltage. Using the ion saturation current from the measured I–V characteristics and making simplifying assumptions about the aluminum plasma allow us to estimate the plasma density. The axial density profile of this plasma plug is shown in Fig. 5. As expected, it is found that the plasma density is proportional to the PFN charging voltage over a range up to 2.5 kV, that is, it is proportional to the cathodic arc current. The measurements show that the plasma density along the axis is peaked, $10^{11}\,\mathrm{cm}^{-3}$, at the location of the pair of entry ports where the plasma enters the beam line and drops off over a distance of a few centimeters.

4.1. RF volume plasma source

The RF pulsed plasma source [32] as shown in the Fig. 4(c) has a six-way cross at the center of its design. A turbo-pump attached to one face maintains the vacuum, while the gas inlet and the

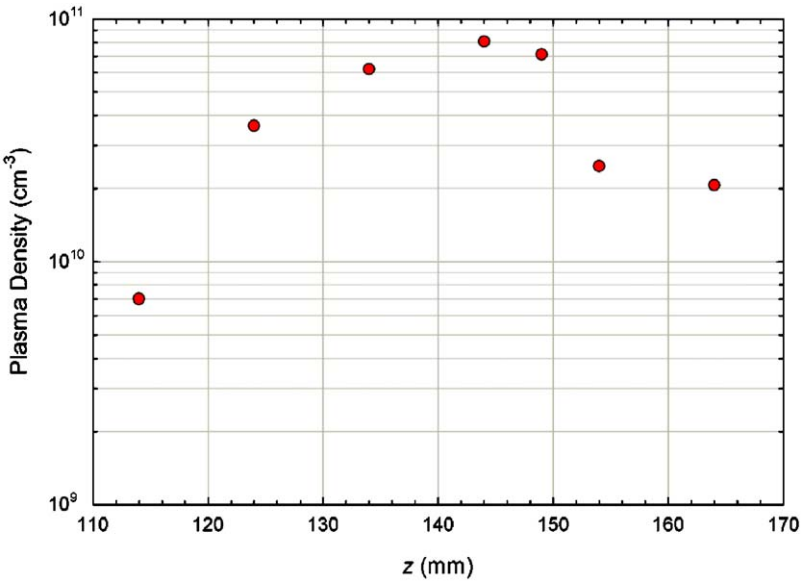

Fig. 5. The axial profile of the plasma density is peaked near the location of the plasma entry ports at 144 mm.

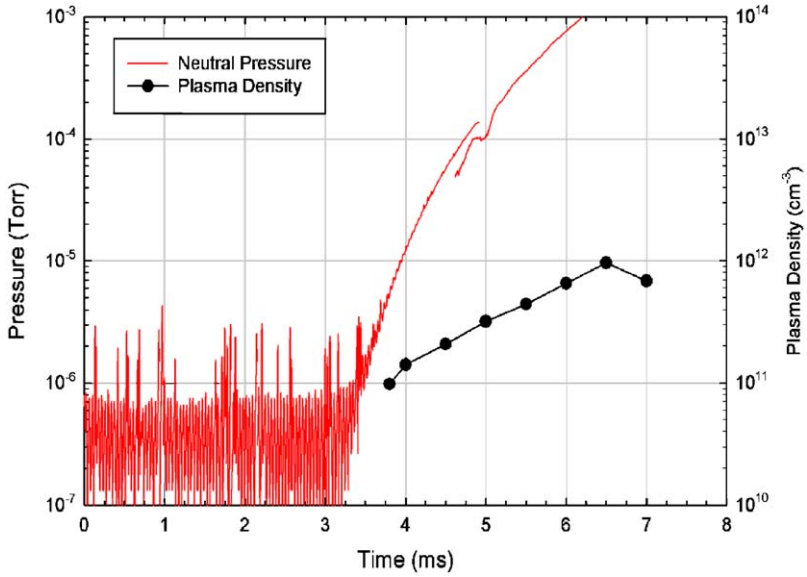

Fig. 6. RF volume plasma density as a function of pressure and time.

RF quartz window are attached to the opposite face. A three-turn copper spiral antenna is situated inside a shielded box and faces the window. The RF matching network is directly connected to the antenna enclosure and is tuned to match the low-impedance antenna to the 50 W transmission cable. Perpendicular to the turbo-pump as well as antenna and directed into the page, are two flanges to the six-way cross where the drift tube for the ion beam is connected. The plasma drifts into the center of the cross and intersects the propagating ion beam. The source operates by applying a puff of argon gas and a pulse of RF power to the antenna. The potential advantages of pulsed operation are that it can easily operate at high peak RF power levels, and the amount of gas can be limited. The plasma density and the neutral gas pressure are issues primarily during the 10 ms the ion beam passes through the plasma. Consequently, plasma parameters and neutral gas pressure are dynamic quantities and have been measured as a function of time in order to evaluate source operation.

The gas valve and the RF power are triggered at the same time ($t = 0$). The source characteristics for a net forward power was ~3.5 kW. Before $t =$ 3.75 ms, the plasma density is less than the sensitivity of the Langmuir probe ($\sim 10^7\,\mathrm{cm}^{-3}$), and the neutral pressure is below the sensitivity of the dynamic pressure measurement (10^{-6} Torr). At $t = 3.75$ ms, the electron density is $10^{11}\,\mathrm{cm}^{-3}$ with simultaneous low neutral pressure. At later times the power density was not sufficient to sustain the ionization fraction, and the neutral density rises faster than the electron density. A profile measurement was made transverse to the axis of the plasma source and turbo-pump as shown in the Fig. 6. The density is peaked on axis. There is a factor of 2 drop near the plasma source wall radius of 5 cm. Distances greater than 5 cm from the center of the cross are hidden from the straight-line path of the plasma out of the source. There the density decreases by an order-of-magnitude at a distance 5 cm from the wall radius of the plasma source. Another profile measurement was made in the six-way cross, but along the axis of the plasma source. In this direction, the plasma has a steep gradient away from the antenna because of the short plasma skin depth (~1 cm).

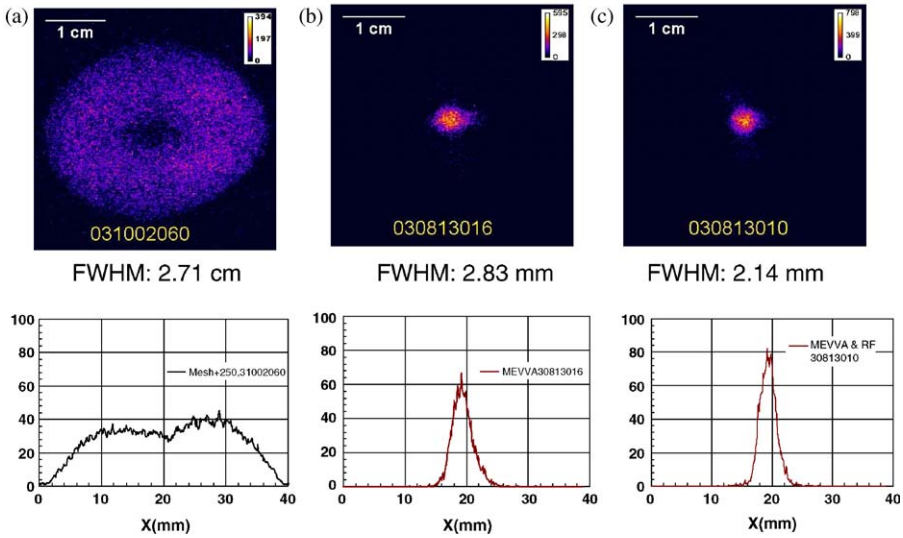

Fig. 7. Beam images at the focal plane for three cases of space-charge neutralization for a high perveance (6×10^{-4}) 24 mA 254 keV K^+ ion beam: (a) non-neutralized, (b) Plasma plug neutralized and (c) plasma plug and RF volume plasma neutralized.

5. Beam neutralization

Non-neutralized and neutralized beams were monitored at the end of 1 m long neutralization drift section (Fig. 1) on a glass or ceramic (96% alumina) scintillator. Charge neutralization of this scintillator was provided by a high-transparency (80–90% transmission) metallic mesh placed on or near the surface of the scintillator. By applying a negative bias to the mesh, stray external electrons were decelerated and deflected away from the scintillator, limiting their contribution to the optical image to negligible levels. Time-resolved beam-induced images on the scintillator screen were captured with a Roper Scientific gated intensified CCD camera viewing the scintillator through a vacuum window, and images were processed using the public-domain program Image J. Fig. 7 shows beam images of a neutralization experiment: (a) non-neutralized, (b) plasma plug, i.e. MEVVA-plasma-neutralized, and (c) plasma plug and RF volume plasma neutralized. A size of 27 mm at Full-Width at Half-Maximum (FWHM) was measured for a non-neutralized condition. The beam radius of 14.7 mm (for Fig. 7(a)) was measured using 1/e lower cutoff statistical deduction from the peak fluence of beam imaged with Image J. A size of 2.83 mm at FWHM was measured for the MEVVA plug neutralization and its radius of 1.6 mm was measured using the same method. A spot size of 2.14 mm at FWHM and 1.3 mm neutralized beam radius were measured for MEVVA plug and volume plasma neutralization. A better-than-90% beam size reduction was measured using plasma sources. Neutralization with a lower perveance, 6 mA beam current using 1 cm aperture instead of 2 cm diameter aperture, was also performed. Fig. 8(a) shows beam images of experimental data for plasma plug neutralized (column 1), plasma plug and RF volume plasma neutralized (column 2), completely neutralized, using pinhole scan (column 3) and numerical results of all these cases (columns). Fig. 8(b) shows numerical simulation of all of these cases 8(a). Results of the 2 different aperture cases (24 and 6 mA) show that neutralized beam sizes did vary significantly with variable perveance.

In the NTX experiment, it was observed that (Fig. 9) there is a decrease in the neutralized beam size as the convergence angle is increased. Eventually, as the angle is increased emittance growth

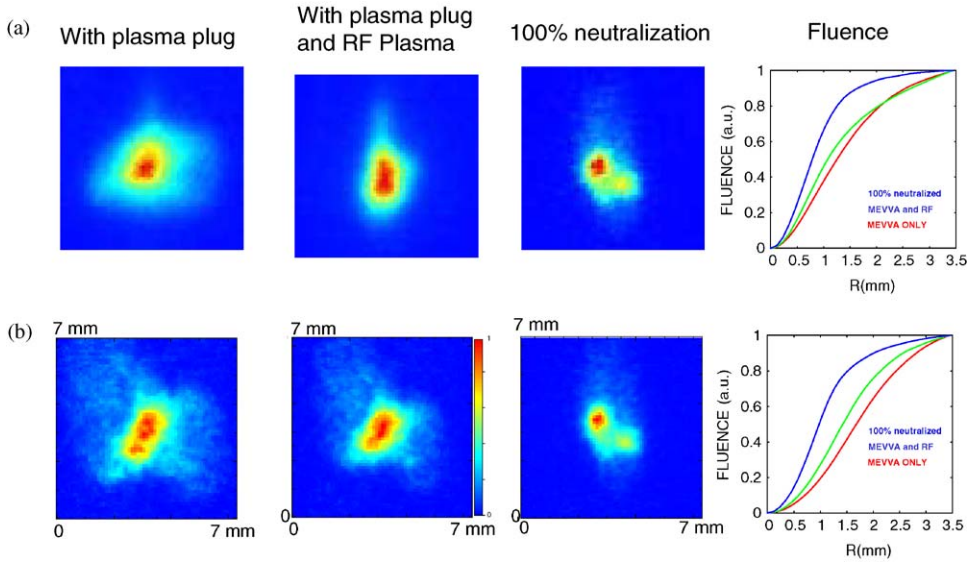

Fig. 8. Theory and calculation (a) from experimental measurements and (b) simulation.

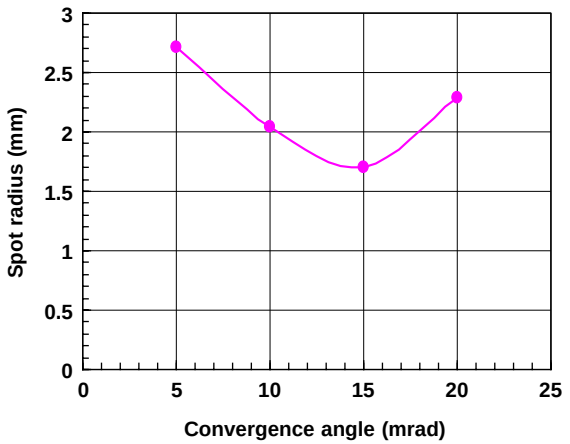

Fig. 9. Spot size depending on convergence angle.

from geometric aberrations increase spot size. Simulation [33] also shows the same behavior.

Neutralized beam spot size variation was also measured by varying scintillator position over a range of around 15 cm, varying beam energies (produced by using the Marx crowbar pulse system), varying MEVVA plug discharge voltage and varying time delay of image recording for head-to-tail of a beam. Fig. 10 shows MEVVA-plug neutralized beam radius as a function of (a) axial focal point position, (b) beam energy variation, (c) MEVVA discharge voltage variation and (d) head-to-tail variation. For the energy variation, sensitivity to chromatic variation is a result of magnetic quadrupole optics.

Simulations [28] of beam dynamics when the plasma plug is present show that if electrical connection is maintained to the pipe wall through electron space charge limited emission (SCLE), the beam spot shows little variation for plasma densities ranging from 3×10^{8} to $3\times10^{10}\,\mathrm{cm}^{-3}$ for an initial plasma temperature of 3 eV. For a 6 eV initial plasma temperature, which is greater than the trapping potential $1/2m_e v_i^2$, the beam spot size was roughly 50% larger than the case with 3 eV plasma. The sensitivity of the beam spot to incoming beam emittance is calculated to be weak, with only a 30% spot-size variation for a factor of three change in emittance. This low sensitivity to emittance indicates that charge neutralization in the NTX experiment should be quite close to the 96% value seen in simulations and not influenced by details in the emittance.

To ascertain the head-to-tail variation of the pulse, a 255 keV beam was transported through a plasma produced with 2 keV discharge potential. Time slices of 100 ns width were recorded with 253

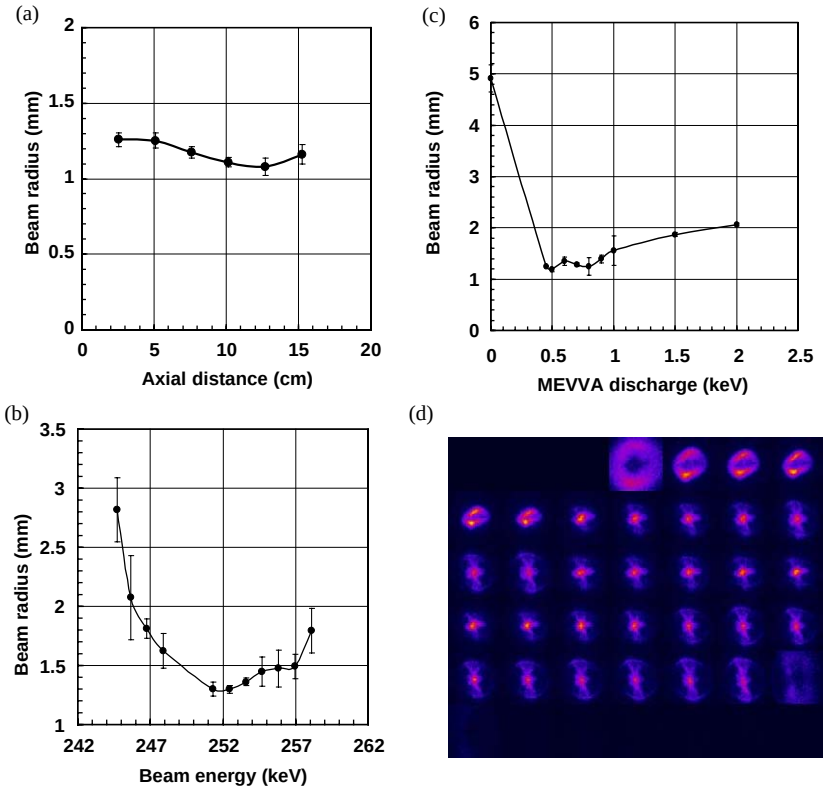

Fig. 10. Beam envelope variations in the (a) axial position, (b) energy variation, keeping quadrupole strength fixed (c) MEVVA discharge voltage and (d) head-to-tail variation.

gain and delays between 4.6 and 12.8 μs in intervals of 0.2 μs. It was observed that the beam head and tail have halos. We inferred that the longitudinal forces due to beam space charge were increasing the velocity of beam head and slowing the beam tail. Although the beam radius looks flat for time delay of 6 to 11μs, closer examination shows that the beam radius variation was of order 0.2 mm. This might be due to shot-to-shot variation of Marx voltage or variation of charge accumulation in the capacitor tank of the MEVVA plasma plug high voltage system.

6. Conclusion

Several experiments have recently been carried out on the Neutralized Transport Experiment (NTX) at Lawrence Berkeley National Laboratory. We have demonstrated experimentally that without neutralization, the 24 mA NTX beam radius at the nominal 1 m focal distance has a 1σ radius of 14.7 mm. When the NTX beam is neutralized by passing it through MEVVA plasma plug and pulse RF volumetric plasma source, the beam 1σ radius decreases to ~1.3 mm. Neutralized beam size depends on convergence angle, beam energy, axial position, and head-to-tail variation of beam parameters, but not significantly on perveance variation. Finally, experiments have shown that the variation of NTX beam quantities matches theoretical predictions.

Acknowledgments

The authors are grateful to all the scientific members and technical staff of the Heavy Ion

Fusion Virtual National Laboratory (HIF-VNL). This work was performed under Contracts No. W-7405-ENG-48 and DE-AC-3-76SF00098 under the auspices of the US Department of Energy by University of California, Lawrence Livermore National Laboratory and Lawrence Berkeley National Laboratory.

References

[1] W.B. Herrmannsfeldt, private communications. ERDA summer study of heavy ions for inertial fusion, R.O. Bangerter, W.B. Herrmannsfeldt, D.L. Judd, L. Smith (Eds.), LBL-5543, California, 1976, p. 25.
[2] See National Technical Information Service Documents Conference no. 780979. (S.S. Yu, H.L. Buchanan, E.P. Lee, F.W. Chambers, in: R.C. Arnold (Ed.), Proceedings of the Heavy Ion Fusion Workshop, ANL-79-41, 1978, p. 403). Copies may be ordered from the National Technical Information Service, Springfield, VA 22161.
[3] See National Technical Information Service Documents Conference no. 791012. (C. L. Olson, in: Proceedings of the Heavy Ion Fusion Workshop, Berkeley, California, 1979, W.B. Herrmannsfeldt (Ed.), LBL-10301, SLAC-PUB-2575, UC-28, 1980, p. 403). Copies may be ordered from the National Technical Information Service, Springfield, VA 22161.
[4] N. Barboza, Fusion Eng. Des. 32–33 (1996) 453.
[5] D.A. Callahan, Fusion Eng. Des. 32–33 (1996) 44.
[6] B.G. Logan, D.A. Callahan, Nucl. Instr. Meth. A 415 (1998) 468.
[7] J.L. Vay, C. Deutsch, AIP Conf. Proc. 406 (1997) 267.
[8] W.M. Sharp, D.A. Callahan-Miller, R.B. Langdon, M.S. Armel, Bull. Am. Phys. Soc. 44 (7) (1999) 201.
[9] I.D. Kaganovich, G. Shvets, E. Startsev, R.C. Davidson, Phys. Plasmas 8 (2001) 4180.
[10] D.V. Rose, D.R. Welch, B.V. Oliver, R.E. Clark, W.M. Sharp, A. Friedman, Nucl. Instr. and Meth. A 464 (2001) 299.
[11] D.R. Welch, D.V. Rose, B.V. Oliver, R.E. Clark, Nucl. Instr. and Meth. A 464 (2001) 134.
[12] S.S. Yu, W.R. Meier, R.P. Abbott, et al., Fusion Sci. Technol. 44 (2003) 266.
[13] T.P. Hughes, R.E. Clark, S.S. Yu, Phys. Rev. ST Accel. Beams 2 (1999) 110401.
[14] D.R. Welch, D.V. Rose, B.V. Oliver, R.E. Clark, Nucl. Instr. and Meth. A 464 (2001) 134.
[15] D.A. Callahan-Miller, M. Tabak, Nucl. Fusion 39 (1999) 883.
[16] C.L. Olson, et al., Proceedings of the 16th International Atomic Energy Agency Fusion Energy Conference 195 (1996).
[17] D.R. Welch, C.L. Olson, Fusion Eng. Des. 32–33 (1996) 477.
[18] D.R. Welch, D.V. Rose, B.V. Oliver, T.C. Genoni, R.E. Clark, C.L. Olson, S.S. Yu, Phys. Plasmas 9 (2002) 2344.
[19] C.L. Olson, Chamber Transport, Proceedings of the 13th International Symposium on HIF, San Diego, CA, March 13–17, 2000, p. 118.
[20] C.L. Olson, et al., Proceedings of 1979 Heavy Ion Fusion Workshop LBL-10301 (1980), P403.
[21] E. Henestroza, S. Eylon, P.K. Roy, S.S. Yu, et al., Physical Review Special Topics—Accelerator and Beams 7 (2004) 083501.
[22] D. Baca, J.W. Kwan, J.K. Wu, in: J. Chew, P. Lucas, S. Webber (Eds.), Proceedings of the 2003 Particle Accelerator Conference, IEEE, USA, 2003, p. 3294.
[23] W.M. Fawley, T. Garvey, S. Eylon, E. Henestroza, A. Faltens, T.J. Fessenden, K. Hahn, L. Smith, D.P. Grote, Phys. Plasmas 4 (1997) 880.
[24] D. Shuman, S. Eylon, E. Henestroza, P.K. Roy, W. Waldron, S.S. Yu, T. Houck, in: J. Chew, P. Lucas, S. Webber (Eds.), Proceedings of the 2003 Particle Accelerator Conference, IEEE, USA, 2003, p. 2628.
[25] P.H. Stoltz, M.A. Furman, J.-L. Vay, A.W. Molvik, R.H. Cohen, Phys. Rev. ST Accel. Beams 6 (2003) 054701.
[26] R.E. Kirby, F.K. King, Nucl. Instr. and Meth. A 469 (2001) 1.
[27] G.F. Dionne, J. Appl. Phys. 44 (1973) 5361.
[28] P.K. Roy, S.S. Yu, S. Eylon, E. Henestroza, et al., Phys. Plasmas 11 (2004) 2890.
[29] I.G. Brown, Rev. Sci. Instrum. 65 (1994) 3061.
[30] R.A. MacGill, M.R. Dickinson, A. Anders, O.R. Monteiro, I.G. Brown, Rev. Sci. Instrum. 69 (1998) 801.
[31] A. Anders, Surf. Coat. Technol. 120–121 (1999) 319.
[32] P. Efthimion, R.C. Davidson, E. Gilson, L. Grisham, in: J. Chew, P. Lucas, S. Webber (Eds.), Proceedings of the 2003 Particle Accelerator Conference, IEEE, USA, 2003, p. 2661.
[33] S.S.Yu, NTX, HIF-VNL Review, LBNL, August 22, 2001.